CAMBRIDGE
UNIVERSITY PRESS

Article
Special Issue dedicated to Peter Williams

Gold and aurostibite from the metaturbidite-hosted Au–Zn–Pb–Ag Hera deposit, southern Cobar Basin, central NSW, Australia: geochemical and textural evidence for gold remobilisation

Ian T Graham[1]* , Adam McKinnon[2], Angela Lay[1,3], Karen Privat[1,4] , Khalid Schellen[1,5], Lachlan Burrows[1,5], Elizabeth Liepa[1] and Hongyan Quan[1]

[1]Earth and Sustainability Sciences Research Centre, School of Biological, Earth and Environmental Sciences, UNSW Sydney, Sydney, NSW 2052, Australia; [2]Aurelia Metals Limited, Level 17, 144 Edward Street, Brisbane, QLD 4000, Australia; [3]Autoridade Nacional de Petroleo e Minerals (ANPM) – Mineral Directorate, Municipio de Dili, Timor-Leste; [4]Electron Microscope Unit, Mark Wainwright Analytical Centre, UNSW Sydney, Sydney, NSW 2052, Australia and [5]Alkane Resources Limited, Level 4, 66 Kings Park Road, West Perth, WA 6005, Australia

Abstract

The Devonian Hera metaturbidite-hosted polymetallic Au–Zn–Pb–Ag deposit of central NSW, Australia, contained a total undepleted resource of 3.6 Mt @ 3.3 g/t Au, 25 g/t Ag, 2.6% Pb and 3.8% Zn. The deposit comprises a number of distinctive lodes with each containing a distinctive ore and alteration/gangue mineralogy, though generally the sulfide ore comprises various mixtures of sphalerite, galena, chalcopyrite, pyrrhotite and relatively common visible gold–electrum. The North Pod and Far West lodes are distinctly Sb rich and contain a more diverse ore mineralogy with arsenopyrite, native silver, native antimony, gudmundite, tetrahedrite-(Fe), argentotetrahedrite-(Fe), acanthite, dyscrasite, nisbite and breithauptite. From analysis of 52,760 assays from across the deposit it was found that there was a very poor correlation between gold and each of Fe, Zn, S, Pb, Cu, As and Ag, whereas Ag correlated reasonably well with both Pb and Zn. Results from EPMA shows that gold varies widely in composition from host-rock associated gold (96 wt.% Au) through more intermediate compositions (88–73 wt.% Au) to electrum (46–27 wt.% Au), commonly associated with Sb-phases and containing significant Sb within the gold itself (1.05–2.58 wt.% Sb). From the Far West lense, aurostibite occurs as distinctive rims around gold. Although aurostibite associated with gold contains no silver, the gold itself contains constant moderate amounts (10.87–12.27 wt.% Ag). We suggest that the aurostibite and other Sb phases formed from a late-stage Sb-rich hydrothermal during low-temperature retrograde skarn alteration. There is abundant evidence for both chemical and physical remobilisation at Hera and this remobilisation is largely responsible for the spectrum of gold compositions observed. The source for these fluids may be an underlying magmatic body, evidence for which occurs as granite pegmatite dykes in various locations throughout the deposit. Furthermore, gold with a moderate to high Sb content may be indicative of a low temperature of formation.

Keywords: gold, aurostibite, remobilisation, Hera mine, orogenic, Cobar Basin, retrograde skarn, antimony

(Received 10 February 2022; accepted 29 April 2022; Accepted Manuscript published online: 12 May 2022; Associate Editor: Stuart Mills)

Introduction

The chemistry and morphology of native gold are of great importance to better understand the genesis and evolution of gold in gold deposits, especially in relation to other associated metals. Gold occurs in a wide variety of economic deposits that have formed in a range of tectonic settings and over a wide range of crustal depths and temperatures. The morphology and chemistry of alluvial or placer gold grains have been used widely in mineral exploration to help determine their likely primary source (e.g.

Fisher, 1945; Knight *et al.*, 1999; Townley *et al.*, 2003; Hough *et al.*, 2009). In addition, gold can be transported in a wide range of fluids/melts and be precipitated from these via a range of mechanisms (Chapman *et al.*, 2009; Frimmel, 2014).

Native gold almost always occurs as an alloy with silver as gold and silver have the same atomic radius and thus can form a continuous alloy series (Hough *et al.*, 2009). Gold can also alloy with a number of other metals including copper, mercury lead, tin, antimony, bismuth and platinum-group elements (Desborough, 1970; Boyle, 1979; Morrison *et al.*, 1991; Townley *et al.*, 2003; Hough *et al.*, 2009; Liu *et al.*, 2021), though these occur mostly in minor concentrations and comprise <1 wt.% (Morrison *et al.*, 1991). Although electrum has been defined as a gold–silver alloy in which the silver content exceeds 20% (Harris, 1990) it is not an official mineral species according to the International Mineralogical Association (Pasero, 2022). Instead, if the Ag–Au alloy contains >50 wt.% Ag it would be called silver and

*Author for correspondence: Ian T Graham, Email: i.graham@unsw.edu.au

conversely, if it contains >50 wt.% Au it would be called gold. However, Harris (1990) also pointed-out that the term 'electrum' is normally applied to epithermal and what we now refer to as orogenic deposits where the Au–Ag alloy exhibits a wide range of silver concentrations.

Gold can also occur in a wide variety of mineral species including various alloys where it is combined with antimony, copper, mercury, bismuth, platinum-group elements and, rarely, tin. It also occurs in tellurides, tellurates, sulfides and selenides (Harris, 1990; Missen *et al.*, 2021). Of relevance to this present study is the mineral aurostibite ($AuSb_2$), a member of the pyrite group where gold is alloyed with antimony and was first described by Graham and Kaiman (1952) from the Giant mine at Yellowknife, Northwest Territories and the Chesterville mine of Ontario, Canada, both being quartz-vein hosted orogenic gold deposits (Shelton *et al.*, 2004; Ispolatov *et al.*, 2008). Since then, it has been described from many deposits including, but not restricted to, the quartz-vein hosted orogenic Mobale gold mine, Kivu, Democratic Republic of Congo (Jedwab *et al.* 1992; Milesi *et al.*, 2006), metamorphosed Sulitjelma VMS deposit of northern Norway (Cook, 1992, 1996), quartz-vein hosted orogenic Kharma Sb deposit of Bolivia (Dill *et al.*, 1995), quartz-vein hosted orogenic West Gore Sb-Au deposit of Nova Scotia, Canada (Kontak *et al.*, 1996), hydrothermal quartz-vein hosted Hillgrove gold-antimony deposit of northeastern NSW, Australia (Ashley *et al.*, 2000), intrusion-related Au–Sb A deposit of New Brunswick, Canada (Cabri *et al.*, 2007; Deschenes *et al.*, 2009; Ravenelle *et al.*, 2008; Watters *et al.*, 2008), intrusion-related Darasun deposit of Eastern Transbaikal, Russia (Bryzgalov *et al.*, 2007; Spiridonov *et al.*, 2010), quartz-vein hosted orogenic Passagem de Mariana gold mine, Brazil (Oberthur and Weiser, 2008), carbonaceous clastic sediment-hosted Suzdal gold deposit of eastern Kazakhstan (Kovalev *et al.*, 2009), metamorphosed mafic-ultramafic hosted orogenic Lapa deposit, Abitibi Belt, Canada (Simard *et al.*, 2013; Jebrak *et al.*, 2016), intrusion-related Mokrsko-West gold deposit of the Bohemian Massif, Czech Republic (Zacharias *et al.*, 2014), metavolcanic hosted Pirunkoukku gold occurrence of northern Finland (Novoselov *et al.*, 2015), the Krasna Hora deposit of the Czech Republic (Zacharias and Nemec, 2017), and most recently, the intrusion-related Oleninskoe Au–Ag deposit of the Kola Peninsula, Russia (Kalinin *et al.*, 2019).

In this paper, we describe the mineral associations, textures and chemistry of gold, electrum and aurostibite from a number of associations and ore lenses within the Devonian Hera metaturbidite-hosted polymetallic Au–Zn–Pb–Ag deposit of the southern Cobar Basin, central NSW, Australia. Hera presented an excellent opportunity to study the textures and chemistry of gold as most of the gold is free-milling (i.e. not locked-up as minute inclusions in phases such as pyrite) and relatively coarse-grained. We also provide potential explanations for the occurrence of aurostibite and the almost complete spectrum of gold–electrum compositions from almost pure Au (∼96 wt.%) to electrum with ∼27 wt.% Au.

Location and geological setting

The Hera mine is located within the southern Cobar Basin, some 5 km south of the town of Nymagee in central New South Wales, Australia (Fig. 1). It is a polymetallic deposit containing economic concentrations of gold, lead, zinc and silver with mineralisation starting 240 metres below the surface. Hera had a total undepleted

resource of 3.6 Mt @ 3.8% Zn, 2.6% Pb, 25 g/t Ag and 3.3 g/t Au. The deposit consists of multiple lodes which are structurally offset by a series of faults. These appear to dip west and strike in a NNW direction for over 800 metres in length with economic mineralisation currently identified to 640 metres below the surface (Fig. 2) (McKinnon and Fitzherbert, 2017).

The Cobar Basin is located within the Central subprovince of the Lachlan Orogen and comprises several shelves (Winduck Shelf, Walters Range Shelf and Kopyje Shelf) and troughs (Cobar Trough, Mount Hope Trough and Rast Trough) (Glen, 1991; David, 2008). Active sedimentation occurred within multiple depositional environments from deep-water troughs to shallow-water shelves. It has been suggested that tectonic activity was initiated on the eastern boundary of the basin and migrated to the west during the early Pragian (410.8–407.6 Ma) or late Lochkovian (419.2–410.8 Ma) (Glen *et al.*, 1994).

The basin contains many regional structures due to the many deformational cycles during and after its deposition (Glen, 1990). Glen (1990) separated the Cobar Basin into a series of structural zones where differing geometry and strain were used to differentiate between them. Zone 1 is located on the eastern margin of the basin and underwent the highest strain; Zone 2 is in the central and south-western part of the basin and underwent a lower strain; and Zone 3 is in the north-western part and underwent the least strain. The Hera deposit is located within Zone 1 as are most of the deposits in the region (Glen, 1991).

The inversion of the basin in the mid-Devonian (395–400 Ma) (Glen *et al.*, 1992) caused the reactivation of existing faults and other structures leading to the mobilisation of fluids causing mineralisation across the region. Glen (1990) suggested that the compression occurred in a northeast/southwest direction and that most of the strain was focussed into Zone 1. Extensive metamorphism of varying grades occurred within the Cobar Basin with burial metamorphism being observed across the region. Greenschist-facies metamorphism is also observed which is related to the basin inversion event. However, there are also greenschist- to low-amphibole-facies assemblages which possibly formed from localised magmatism in conjunction with burial gradients until the basin inversion event (Fitzherbert *et al.*, 2017).

The creation of the basin led to the deposition of the various basin related sediments forming the Cobar Supergroup. The sediments deposited within the supergroup vary in their depositional environment with deep-water troughs containing siliciclastics (Cobar Basin) and volcanic–volcaniclastics–siliciclastics (Mt Hope Trough and Rast Tough) and flanking (Kopyje Shelf, Winduck Shelf) and intrabasinal shelfs (Wiltagoona, Walters Range Shelf) (David 2018). The Cobar Trough not only hosts the Hera deposit, but many of the region's mineral deposits (i.e. Peak mine, CSA mine and Great Cobar mine).

The Hera deposit is hosted within the finer-grained sedimentary rocks of the Mouramba Group and overlying Lower Amphitheatre Group (David, 2005). It lies 1 km west of the Rookery Fault, which is steep westward dipping, bounds the eastern margin of the Cobar Basin (David, 2005) and is associated with many of the deposits in the region. The deposit shows a strong structural control being hosted within a fault splay with a NNW-trending cleavage (David, 2005). It is made-up of several steeply west dipping, narrow ore bodies which are split into multiple lenses by two sets of parallel faults, one steeply south dipping set and one steeply east dipping set (McKinnon and Fitzherbert, 2017). Waltenburg *et al.* (2019) obtained consistent U–Pb ages of 383 Ma on euhedral titanite
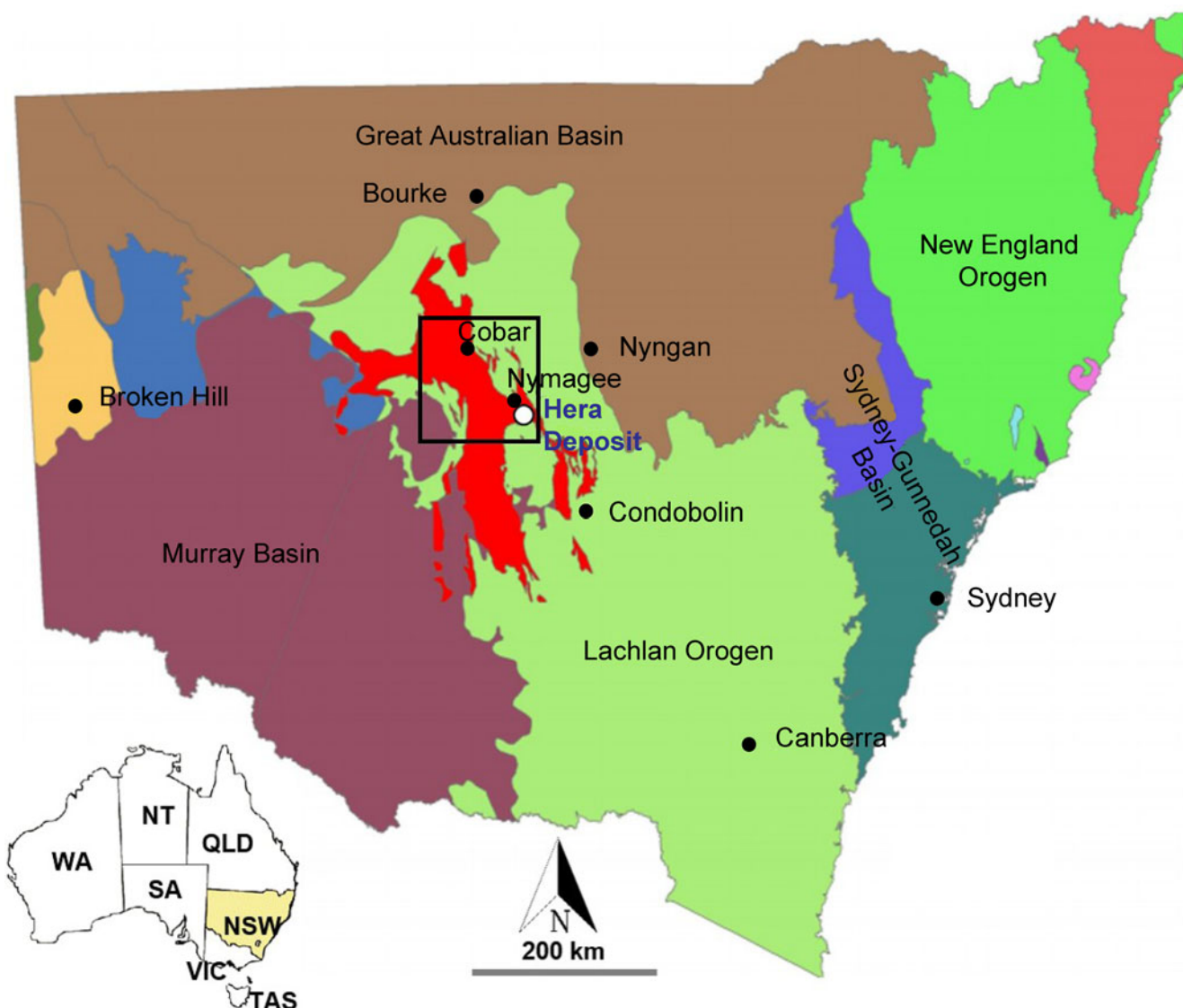
Fig. 1. Map showing the location of the Hera mine (indicated by white circle) and limits of the Cobar Basin (marked in red) within central NSW, Australia (adapted from David, 2006).

crystals from quartz veins from the 435 and 460 levels of the Hera mine and this age is within error of a preliminary Ar–Ar age of 382 Ma for muscovite intergrown with sulfides from the Far West ore zone (Downes and Phillips, 2018).

Fitzherbert *et al.* (2020) described the Hera deposit as a complex distal skarn with two distinct skarn types, a prograde skarn and a retrograde skarn. The prograde skarn comprises two subtypes: (1) silicilastic-hosted veins and breccia-fill hosted within metasiltstones comprising quartz–calcsilicate veins with an assemblage of quartz–garnet (with grossular-rich cores and spessartine-rich rims)–zoisite–titanite–tremolite ± scheelite; (2) sandstone/carbonate replacement skarn hosted primarily within sandstones comprising pods/clasts of grossular–quartz–diopside–actinolite–zoisite–anorthite ± carbonate. The retrograde skarn is ubiquitous throughout many of the sulfide orebodies with a moderate-temperature retrograde assemblage of actinolite–tremolite–biotite ± spessartine followed by a later low-temperature skarn assemblage of chlorite–muscovite. In addition, Fitzherbert *et al.* (2017) suggested that the prograde event occurred at temperatures of ~400–500°C and that the retrograde event occurred at temperatures of 200–250°C.

At Hera, the main ore lenses are Far West, Far West Lower (also called Far West Deeps), Hays North, Hays South, Main North, Main South and North Pod (Fig. 2). Most of the ore comprises sub-massive to massive sulfides, but sulfide veins are also relatively abundant as are breccia ores comprising angular to sub-rounded host-rock clasts in a sphalerite–galena matrix (Graham *et al.*, 2021). The latter are known as 'durchbewegung' (Vokes, 1969), provide clear evidence of remobilised sulfides, and were described from the CSA mine in the north of the Cobar Basin by Gilligan and Marshall (1987). Most of the ore at Hera comprises an early generation of pyrrhotite with minor chalcopyrite with the main ore stage characterised by sphalerite and galena with minor chalcopyrite and pyrrhotite, and rare pyrite and gold (Burrows, 2017; Graham *et al.*, 2021). Visible gold is relatively common within the main sulfide ores, occurring as small (0.5–2mm) grains, most commonly enclosed in sphalerite associated with galena (Fig. 3). However, the Far West and North Pod lenses differ in additionally containing a number of Ag-rich, Sb-rich and As-rich phases including relatively abundant gudmundite (FeSbS), Ag-rich tetrahedrite, freibergite-series
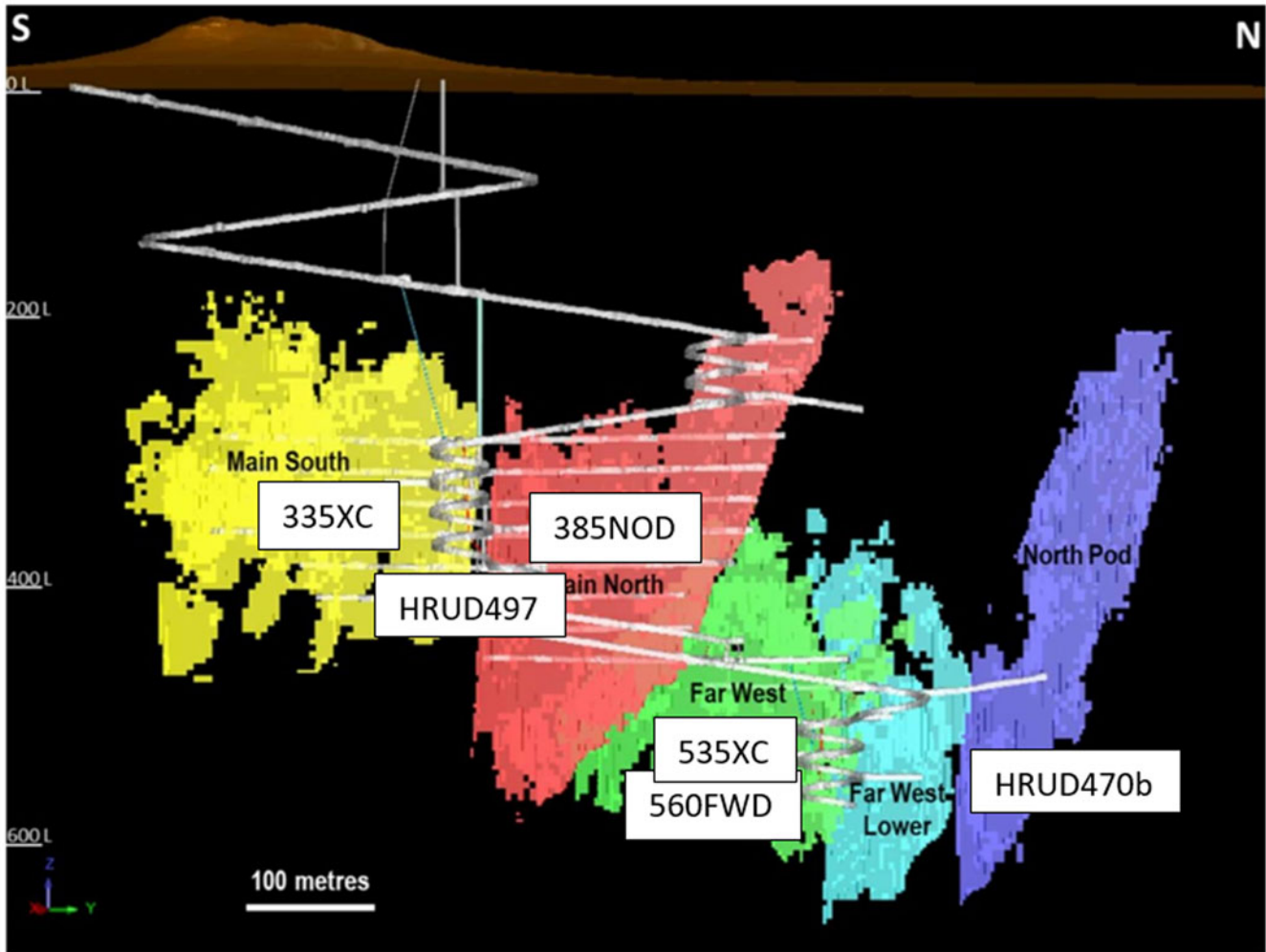
Fig. 2. Cross-section showing the distribution of the various lodes within the Hera mine and location of samples studied (Aurelia Metals Ltd, 2018).

Fig. 3. Hand-specimen image of cut slice of ore from the Hera deposit showing abundant visible gold in sphalerite–galena (scale bar is in mm).

minerals, tetrahedrite and arsenopyrite, along with sporadic occurrences of native silver, dyscrasite (Ag_3Sb), native antimony, acanthite, breithauptite (NiSb) and nisbite ($NiSb_2$) (Lay, 2019; Graham *et al.*, 2021). Using the recent nomenclature and classification for the tetrahedrite group in Biagioni *et al.* (2020), the North Pod contains both argentotetrahedrite-(Fe) and tetrahedrite-(Fe) whereas tetrahedrite from the other lenses at Hera (Main South, Main North, Far West, Far West Deeps) can all be classified as tetrahedrite-(Fe). Fitzherbert *et al.* (2020) briefly described some of the visible gold occurrences from Hera but provided no analyses. They suggested that gold was associated with the retrograde skarn – commonly, but not exclusively, with sulfides (with a distinctive low-Fe sphalerite as infill between breccia clasts) with gold away from the sulfide lenses being often remobilised within the main foliation.

Cobar-style deposits were defined initially by Lawrie and Hinman (1998) who formed a genetic model for these deposits. Cobar-style deposits are some of the richest deposits within the Cobar Basin. They have several characteristics such as narrow steeply-dipping ore lenses which are broken-up *en echelon* by faults (David, 2018). These lenses are massive sulfides typically containing gold and various base metals (i.e. copper, lead and zinc). Past studies initially classified Hera as a Cobar-style deposit

Table 1. Average metal contents for Pb, Zn, Cu, Au, Ag, Fe, S and As from the various lodes of the Hera deposit.

Hera Lode	Pb (wt.%)	Zn (wt.%)	Cu (wt.%)	Au (g/t)	Ag (g/t)	Fe (wt.%)	S (wt.%)	As (ppm)	n^*
Far West	2.3	4.0	0.1	3.2	13	4.1	3.1	42	10,784
Far West Deeps	1.7	2.5	0.1	4.6	13	4.2	2.3	50	6906
Hays North	1.7	2.7	0.0	4.4	6	3.7	2.1	23	141
Hays South	1.1	1.9	0.1	7.5	7	3.6	2.1	30	914
Main North	1.9	3.0	0.1	3.8	10	4.1	2.9	19	8579
Main South	2.4	2.8	0.2	3.9	11	4.7	3.5	34	7823
North Pod	2.4	3.0	0.1	2.8	32	5.3	3.4	590	17,613
Total	2.2	3.1	0.1	3.5	19	4.6	3.1	221	52,760

*n = number of samples analysed.

(David, 2005) due to its similarities to other such deposits. However, recent studies have found characteristics within the Hera deposit that conflict with some of these criteria (Burrows, 2017; Lay *et al.*, 2018; Lay, 2019; Schellen 2019, 2020; Graham *et al.*, 2021). Hera contains the same initial mineralisation stages as other Cobar-style deposits with an initial stage during basin inversion and a second stage of mineral replacement. However, a third stage of skarn mineralisation was also found to occur across most of the ore bodies, characterised by widespread tremolite, commonly intergrown with sulfides (Burrows, 2017), suggesting an additional event occurring after the initial two mineralisation events. Unusual elemental associations are also noted with gold being abnormally high (Lay *et al.*, 2018) as well as elevated levels of antimony and silver within the North Pod (Lay, 2019). There is also clearly more than one epigenetic gold mineralisation event and abundant (though non-economic) scheelite mineralisation (Graham *et al.*, 2021).

Sampling and analytical methods

This paper results from five years of study at UNSW Sydney, largely the honours projects of Burrows (2017), Liepa (2019) and Schellen (2020), along with part of the PhD project of Lay (2019), and ongoing studies since by the senior author. The most comprehensive sample collection was made during several trips in 2016–2019, from numerous underground exposures *in situ*, the run of mine (ROM) pad on the surface, and from both underground (HRUD) and surface (HM) diamond drillholes.

All samples were first investigated under reflected light microscopy using a Leica DM2500P polarising microscope at the School of Biological, Earth and Environmental Sciences, UNSW Sydney. These were then analysed for their gold chemistry using the JEOL JXA-8500F Hyperprobe electron probe micro-analyser (EPMA) within the Electron Microscopy Unit (EMU), UNSW. A series of synthetic metals (bismuth for Bi and Cd for cadmium) and natural mineral standards (cobaltite for Co and As; millerite for Ni; galena for Pb and S; chalcopyrite for Cu, Fe and S; sphalerite for Zn; pentlandite for Ni and Fe; and stibnite for Sb) were used as calibration standards. For the gold and silver analyses, two synthetic alloy standards with differing Au:Ag were used, one a commercial supplied refined 24 carat fine gold (i.e. certified 99.9% purity) and the other an alloy of composition $Au_{64}Ag_{36}$ made in the Materials Sciences laboratories at UNSW from the 24 carat gold described above mixed with pure certified silver. A probe current of 10 µA, an accelerating voltage of 25 kV with a focused beam and a 10 s count time were used. Wavelength-dispersive spectroscopy (WDS) elemental mapping of some of the samples was also acquired using the same JEOL instrument with the following operating conditions of 20 kV accelerating voltage, 30 nA beam

current and dwell time of 10 ms per pixel. During the early part of this study, unfortunately only Au and Ag were analysed for and hence the results for these analyses are expressed as Au:Ag ratios. As most of the aurostibite grains were in the small size range of 5–10 µm, there was probably interference in the analyses from surrounding sphalerite and pyrrhotite. Because of this, the analyses presented in the main body of this paper cover the key elements present, Au, Sb, Bi and As, and have been normalised. The original analyses with a full element list are presented in Supplementary Table S1.

Results

Assay results and correlations

Assay results for 52,760 ore samples from the Hera deposit are presented in Table 1. Unfortunately, there are no results for Sb as this was not routinely assayed for as it mostly occurs in trace amounts at Hera. These show that the overall composition of the sulfide ore for Hera comprises 4.6% Fe, 3.1% Zn, 3.1% S, 2.2% Pb, 0.1% Cu, 221 ppm As, 19 g/t Ag and 3.5 g/t Au. However, the results for both Ag and As are strongly skewed by the North Pod, which for the Hera deposit is unusually enriched in these with an average of 32 g/t Ag (rest of deposit mostly ~10 g/t) and 590 ppm As (compared to 19 ppm for the Main North and 50 for the Far West Deeps lenses). Variation also occurs in gold, reaching a maximum in the Hays South (7.5 g/t) and a minimum in North Pod (2.8 g/t). Correlation coefficients were also determined for all elements in the assay data. Overall, these show that Au correlates very poorly with all elements assayed (Table 2), especially for Ag (0.05). Table 3 is a breakdown of the correlation coefficients for each of the main ore lenses. Once again, these show very poor correlations between Au and the other elements assayed for, with Au having highest correlations with S% for Far West and Far West Deeps (0.18), Ag for both Main North (0.12) and Main South (0.25) lenses, and Cu for the North Pod (0.17). These alone would tentatively suggest that Au at Hera occurs in a number of associations and/or generations.

Gold–electrum textures, mineral associations and chemistry

As shown from the assay data, gold is widespread throughout the Hera deposit. Over the last 5 years of study, a number of distinctive associations have been found to occur. At 385NOD (Main lode), gold occurs in thin discontinuous quartz veinlets associated with minor fine-grained disseminated galena and sphalerite (Fig. 4a). The gold occurs as (1) subhedral equant-shaped grains some 10–50 µm across; (2) platy grains with irregular cuspate-lobate boundaries some 10–250 µm, in places rimmed by either galena or tetrahedrite. Results of EPMA (8 analyses, Table 4)

Table 2. Correlation coefficients (*n* = 52,760) for Pb, Zn, Au, Ag, Cu, S, Fe and As from the Hera deposit (significant correlations marked in bold).

	Pb (wt.%)	Zn (wt.%)	Au (g/t)	Ag (g/t)	Cu (wt.%)	S (wt.%)	Fe (wt.%)	As (ppm)
Pb (wt.%)	1.00							
Zn (wt.%)	**0.82**	1.00						
Au (g/t)	0.11	0.11	1.00					
Ag (g/t)	**0.51**	**0.46**	0.05	1.00				
Cu (wt.%)	0.33	0.16	0.06	0.16	1.00			
S (wt.%)	**0.86**	**0.86**	0.09	**0.52**	**0.48**	1.00		
Fe (wt.%)	0.39	0.24	0.01	0.39	**0.53**	**0.62**	1.00	
As (ppm)	0.13	0.06	−0.03	0.25	−0.03	0.15	0.29	1.00

showed that this is the most Au-rich gold from Hera with 94.28–96.36 wt.% Au, 3.68–3.97 wt.% Ag and 0.46–0.90 wt.% Bi and both As and Sb below the detection limit. As clearly seen from the analyses, there is little variation in gold chemistry from this lense, especially in the Au:Ag ratio (24.27–25.75; Table 4).

From the Far West lense at 560FWD, a rich and complex association of gold with galena, sphalerite, chalcopyrite, pyrrhotite, gudmundite, tetrahedrite and aurostibite was found (Fig. 5a). In this association, the gold occurs as both subhedral equant-shaped grains some 10–50 μm (Fig. 5b) and as cuspate–lobate shaped

Table 3. Correlation coefficients for Pb, Zn, Cu, Au, Ag, Fe, S and As from the Far West and Far West Deeps (*n* = 17,690), Main North (*n* = 8579), Main South (*n* = 7823) and North Pod (*n* = 17,613) lodes of the Hera deposit (significant correlations marked in bold).

Far West and Far West Deeps (*n* = 17,690)

	Pb (wt.%)	Zn (wt.%)	Au (g/t)	Ag (g/t)	Cu (wt.%)	S (wt.%)	Fe (wt.%)	As (ppm)
Pb (wt.%)	1.00							
Zn (wt.%)	**0.89**	1.00						
Au (g/t)	0.16	0.18	1.00					
Ag (g/t)	0.26	0.22	0.08	1.00				
Cu (wt.%)	0.25	0.13	0.01	0.12	1.00			
S (wt.%)	**0.92**	**0.94**	0.18	0.25	0.38	1.00		
Fe (wt.%)	0.21	0.11	0.08	0.12	**0.66**	0.36	1.00	
As (ppm)	−0.01	−0.02	−0.02	0.03	0.00	−0.01	0.10	1.00

Main North (*n* = 8579)

	Pb (wt.%)	Zn (wt.%)	Au (g/t)	Ag (g/t)	Cu (wt.%)	S (wt.%)	Fe (wt.%)	As (ppm)
Pb (wt.%)	1.00							
Zn (wt.%)	**0.73**	1.00						
Au (g/t)	0.10	0.15	1.99					
Ag (g/t)	**0.63**	0.40	0.12	1.00				
Cu (wt.%)	0.37	0.002	−0.001	0.44	1.00			
S (wt.%)	**0.81**	**0.66**	0.09	0.62	**0.65**	1.00		
Fe (wt.%)	0.39	0.16	−0.015	0.44	**0.82**	**0.70**	1.00	
As (ppm)	−0.06	−0.06	0.02	0.07	−0.04	−0.06	0.01	1.00

Main South (*n* = 7823)

	Pb (wt.%)	Zn (wt.%)	Au (g/t)	Ag (g/t)	Cu (wt.%)	S (wt.%)	Fe (wt.%)	As (ppm)
Pb (wt.%)	1.00							
Zn (wt.%)	**0.77**	1.00						
Au (g/t)	0.20	0.20	1.00					
Ag (g/t)	**0.85**	**0.67**	0.25	1.00				
Cu (wt.%)	**0.51**	0.29	0.12	**0.51**	1.00			
S (wt.%)	**0.81**	**0.71**	0.20	**0.76**	**0.69**	1.00		
Fe (wt.%)	0.25	−0.05	0.06	0.30	**0.59**	**0.62**	1.00	
As (ppm)	0.06	0.10	0.02	0.09	−0.02	0.02	−0.05	1.00

North Pod (*n* = 17,613)

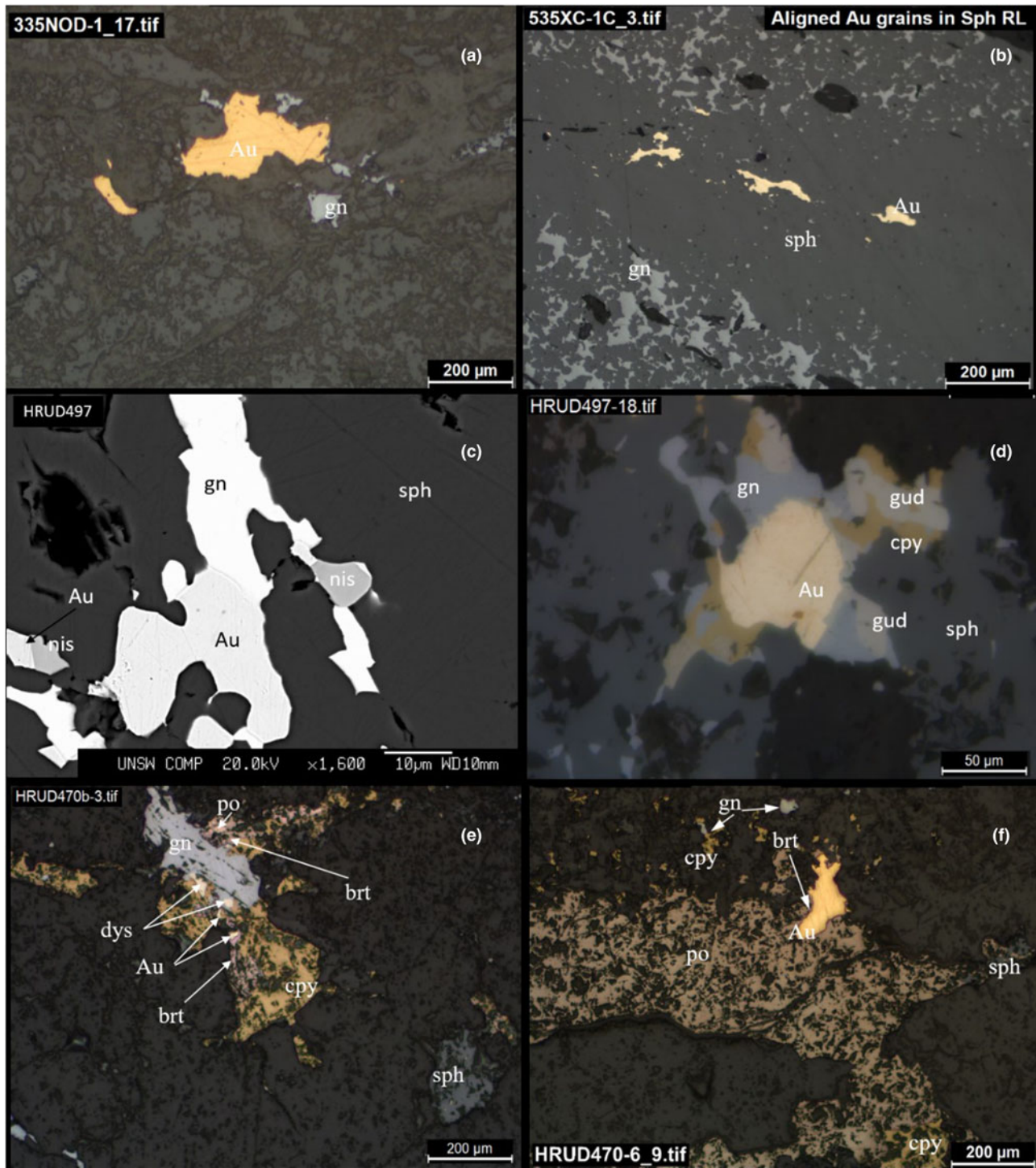|	Pb (wt.%)	Zn (wt.%)	Au (g/t)	Ag (g/t)	Cu (wt.%)	S (wt.%)	Fe (wt.%)	As (ppm)
Pb (wt.%)	1.00							
Zn (wt.%)	**0.85**	1.00						
Au (g/t)	0.05	−0.01	1.00					
Ag (g/t)	**0.72**	**0.74**	0.02	1.00				
Cu (wt.%)	0.34	0.31	0.17	0.26	1.00			
S (wt.%)	**0.87**	**0.95**	0.02	**0.75**	0.43	1.00		
Fe (wt.%)	**0.57**	**0.62**	0.04	**0.56**	0.45	**0.76**	1.00	
As (ppm)	0.17	0.11	−0.03	0.21	−0.03	0.17	0.25	1.00

Fig. 4. Photomicrographs of various gold occurrences and their associations within the ore lenses of the Hera deposit in reflected light and back-scattered electron images: (a) native Au within fracture associated with galena within host siltstone from Main Lode; (b) aligned platy electrum grains within cross-cutting sphalerite vein from Far West Deeps ore lens; (c) nisbite associated with electrum and galena within sphalerite from the Central South; (d) electrum rimmed by galena, gudmundite and chalcopyrite within sphalerite from Central South; (e) dyscrasite rimming galena associated with chalcopyrite and electrum rimmed by breithauptite from North Pod; and (f) breithauptite enclosed in electrum rimmed by pyrrhotite from North Pod. Key: Au – gold; brt – breithauptite; cpy – chalcopyrite; dys – dyscrasite; gn – galena; gud – gudmundite; nis – nisbite; po – pyrrhotite; and sph – sphalerite.

grains associated with galena and sphalerite ranging widely in size from <10 μm to 1 mm (Fig. 5c). The gold grains are commonly rimmed by both aurostibite (see below) and tetrahedrite (Fig. 5d). The gold grains from this lense are relatively Au rich (11 analyses, Table 4), comprising 86.44–87.76 wt.% Au, 10.87–

12.27 wt.% Ag and 0.44–0.55 wt.% Bi with both As and Sb being below detection limit. As with the gold grains from 385NOD, there is little variation in the gold chemistry from this lense with the Au:Ag ratio varying little from 7.15–8.03 (Table 4).

Table 4. EPMA (wt.%.) of gold-electrum from the Hera mine, – = below detection limit.

Au	Ag	As	Bi	Sb	Total	Au:Ag
Ore body: Far West; Sample 560FWD						
86.68	11.89	–	0.49	–	99.06	7.29
87.76	12.27	–	0.46	–	100.49	7.15
86.86	11.66	–	0.46	–	98.98	7.45
86.51	11.58	–	0.52	–	98.61	7.47
86.46	11.77	–	0.45	–	98.68	7.34
86.44	11.64	–	0.48	–	98.56	7.43
86.64	11.45	–	0.55	–	98.64	7.57
87.25	11.04	–	0.44	–	98.73	7.90
87.24	10.87	–	0.49	–	98.60	8.03
87.02	11.10	–	0.49	–	98.61	7.84
86.62	11.46	–	0.48	–	98.56	7.56
Ore body: Main; Sample: 385NOD2						
94.28	3.78	–	0.46	–	98.52	24.94
94.76	3.68	–	0.55	–	98.99	25.75
94.88	3.70	–	0.74	–	99.32	25.64
95.11	3.81	–	0.57	–	99.49	24.96
94.31	3.73	–	0.59	–	98.63	25.28
95.85	3.74	–	0.41	–	100.00	25.63
95.77	3.80	–	0.90	–	100.47	25.20
96.36	3.97	–	0.52	–	100.85	24.27
Ore body: North Pod; Sample: HRUD470b						
28.25	69.91	–	–	2.19	100.35	0.40
37.13	62.48	–	0.10	1.18	100.89	0.59
36.84	62.56	–	0.31	1.05	100.76	0.59
27.42	70.98	–	0.10	2.49	100.99	0.39
27.66	70.60	0.05	0.22	2.58	101.11	0.39
28.61	70.25	–	0.20	2.26	101.32	0.41
37.55	62.34	0.02	0.23	1.10	101.24	0.60
28.52	70.23	0.03	0.22	2.27	101.27	0.41
28.26	69.44	–	0.17	2.27	100.14	0.41
36.95	62.68	0.02	0.25	1.44	101.34	0.59
26.77	71.70	–	0.26	2.71	101.44	0.37
29.01	70.02	0.06	0.24	2.07	101.40	0.41
Ore body: Central South; Sample: HRUD497						
41.33	57.12	0.03	0.37	1.68	100.53	0.72
41.72	57.24	–	0.26	1.80	101.02	0.73
41.72	57.49	0.04	0.24	1.66	101.15	0.73
42.20	57.02	–	0.23	1.70	101.15	0.74

Samples from the North Pod (HRUD470b) are very Ag rich and hence are here called electrum. These grains occur in a complex Sb-rich polymetallic association with dyscrasite, breithauptite, galena, sphalerite, pyrrhotite and chalcopyrite (Figs 4e and f). Gold occurs as both subhedral equant-shaped grains ranging in size from <1 to 25 μm and as larger cuspate-lobate grains some 50–200 μm and commonly rimmed by pyrrhotite. There is a large variation in the chemistry of electrum with 26.77–37.55 wt.% Au, 62.34–71.70 wt.% Ag, below detection limit (bdl)–0.06 wt.% As, bdl–0.31 wt.% Bi and 1.05–2.58 wt.% Sb (12 analyses, Table 4). Unlike the grains from the other lenses described above, these grains are very Sb rich and have low Au:Ag ratios of 0.37–0.60.

As with the North Pod, samples from the Central South lense (HRUD497) are also Ag rich and hence electrum. These grains also occur in a complex association with galena, sphalerite, gudmundite, chalcopyrite and nisbite (Figs. 4c and d). The gold grains occur as (1) small (10–20 μm) subhedral equant-shaped grains in sphalerite; (2) more elongate to platy grains (10–50 μm) in sphalerite; and (3) as complex intergrowths with galena and nisbite cross-cutting massive sphalerite (Fig. 4c). However, unlike electrum from the North Pod, there is little variation in the chemistry of the electrum with 41.33–42.20 wt.% Au, 57.02–57.49 wt.% Ag, bdl–0.04 wt.% As, 0.23–0.37 wt.% Bi and 1.66–1.80 wt.% Sb (4 analyses, Table 4). As with the North Pod

sample, these grains are also Sb rich and have very consistent Au:Ag ratios of 0.72–0.74 (Table 4).

Early on in this project, grains from 335XC (Main South lode) and 535XC (Far West Deeps lode) were only analysed for their gold and silver and hence will only be used for comparative purposes here. The grains from 335XC were found to be Au-rich electrum with a consistent Au:Ag of 46:54 (Table 5). These occur as cuspate–lobate grains (50–75 μm) associated with a relatively simple base-metal sulfide assemblage of pyrrhotite, galena, sphalerite and chalcopyrite (Fig. 5e). In contrast, grains from 535XC were also found to be gold with Au:Ag varying only slightly from 80:20 to 73:27 (Table 5). These occur in a number of associations including: (1) discrete equant, subhedral-shaped gold grains (10–30 μm) within sphalerite and galena; (2) aligned elongate cuspate–lobate gold grains (<10 to 200 μm) in a sphalerite vein cross-cutting an earlier sphalerite–galena vein (Fig. 4b); and (3) as cuspate–lobate shaped gold grains (<1 to 100 μm) enclosed in massive sphalerite.

Aurostibite

Aurostibite ($AuSb_2$) was only found in 560FWD, though in relative abundance associated intimately with gold, sphalerite and galena. It occurs as both cuspate–lobate shaped aggregates (Figs 6a and b) and as small (10–20 um) subhedral equant-shaped grains, always rimming the associated grains of gold (Figs 6c and d). The aurostibite grains have a relatively constant composition of 42.82–43.68 wt.% Au, 55.78–56.63 wt.% Sb, 0.21–0.28 wt.% As and 0.20–0.34 wt.% Bi (12 analyses, Tables 6 and S1). As discussed above, the associated gold grains are Au rich and contain minor Bi but with both As and Sb being below detection limit.

Discussion

Origin of aurostibite

In their study of the Krasna Hora Sb–Au deposit, Czech Republic, Zacharias and Nemec (2017) found that aurostibite was always later than gold and that the aurostibite contained minor amounts of bismuth (0.11–0.15 wt.%) and tellurium (0.11–0.16 wt.%), with one grain also containing minor silver (bdl–0.5 wt.%) but no arsenic. In a study of the Darasun deposit of Eastern Transbaikalia, Russia, Spiridonov *et al.* (2010) found that aurostibite replacing gold contained substantial bismuth (2.49–4.60 wt.%) and arsenic (1.16–1.4 wt.%) but no silver, while aurostibite pseudomorphing maldonite contained even more bismuth (8.98–9.83 wt.%) but was devoid of both arsenic and silver. Furthermore, Oberthur and Weiser (2008) found that aurostibite from the Passagem de Maria mine, Brazil, was highly enriched in bismuth (11.19–11.57 wt.%) along with minor arsenic (0.43–0.54 wt.%) and was also devoid of silver. The results from this study differ only slightly from these (Tables 6 and S1) with trace amounts of both arsenic (0.21–0.27 wt.%) and bismuth (0.19–0.33 wt.%) in Hera aurostibite in addition to consistent low amounts of nickel (bdl–0.21 wt.%). The low bismuth for Hera is not surprising as the Hera orebody contains very little bismuth and no bismuth minerals have been found.

As with the Krasna Hora deposit and many others where gold is associated with aurostibite (e.g. the Darasun deposit of Eastern Transbaikal, Russia, Bryzgalov *et al.*, 2007; Sulitjelma deposit of northern Norway, Cook *et al.*, 1993; Kharma deposit of Bolivia, Dill *et al.*, 1995; and the Suzdal deposit Eastern Kazakhstan,
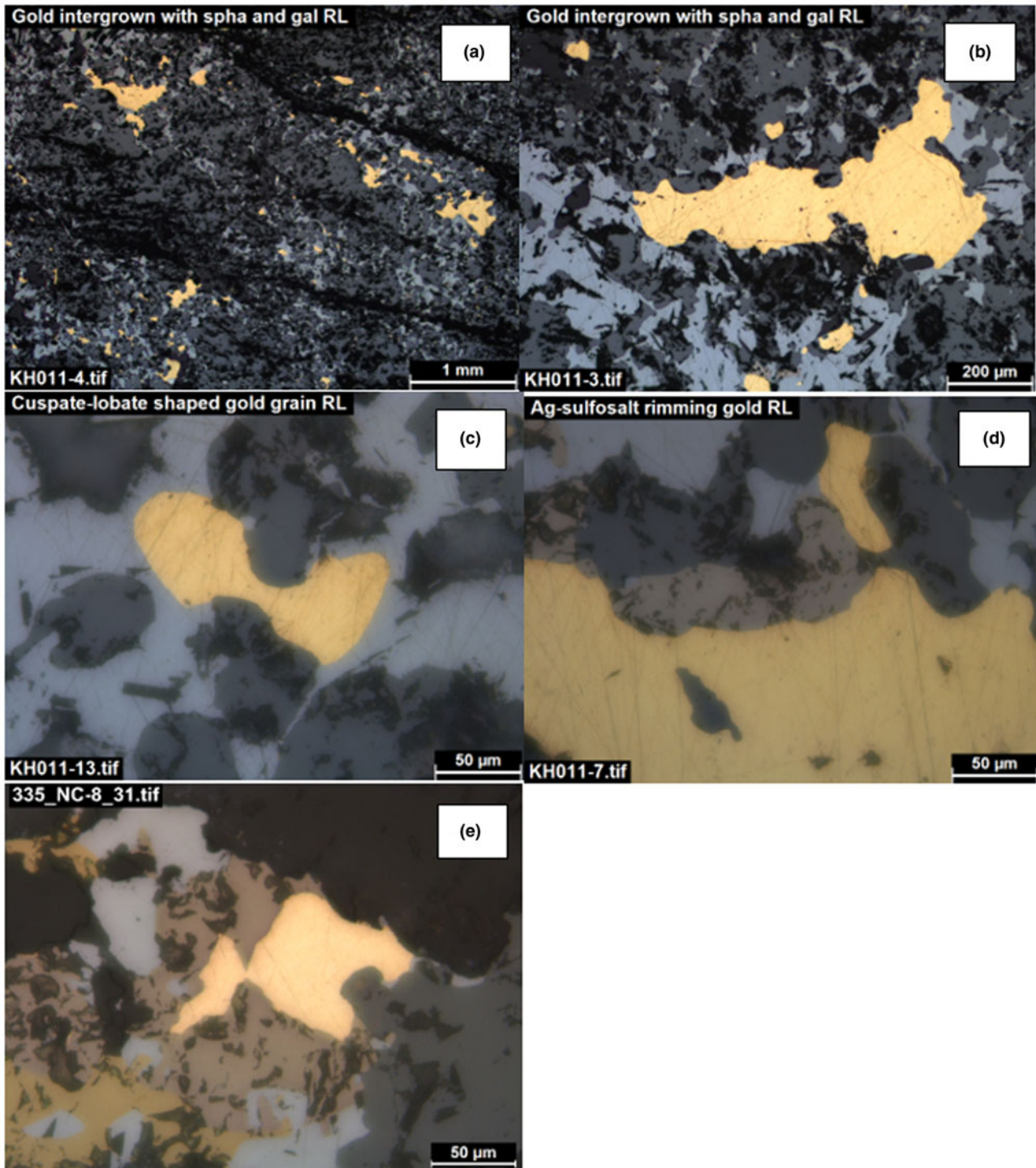
Fig. 5. Photomicrographs in reflected light of various gold occurrences and their associations within selected ore lenses of the Hera deposit: (a) gold intergrown with sphalerite, galena and tremolite from 560 Far West; (b) gold intergrown with sphalerite, galena and tremolite from 560 Far West; (c) cuspate–lobate gold grain with sphalerite and galena from 560 Far West; (d) gold rimmed by tetrahedrite from 560 Far West; and (e) cuspate–lobate gold with pyrrhotite, sphalerite, galena and chalcopyrite from Main South.

Kovalev *et al.*, 2009) aurostibite is always later than gold, occurring as rims around the gold grains (Fig. 6). Collectively, these studies suggest that not only is aurostibite always later than the associated gold, but that its composition can vary widely in terms of its bismuth and arsenic and that it is generally completely devoid of silver. For the Krasna Hora deposit, Zacharias and Nemec (2017) found that the gold grains rimmed by aurostibite were Au rich (90.33–98.2 wt.%), with low to moderate silver (1.99–10.36 wt.%), low antimony (bdl–0.92 wt.%), low bismuth (bdl–0.34 wt.%) and were devoid of arsenic. The gold associated with aurostibite from Hera completely lacked any antimony, contained minor amounts of bismuth and had a relatively constant silver content (10.87–12.27 wt.%; Table 4).

Table 5. Au–Ag ratios for gold-electrum samples from the 335XC and 535XC lodes.

Lode	Au	Ag	Au:Ag
335XC	46	54	0.85
	46	54	0.85
	46	54	0.85
535XC	80	20	4.00
	79	21	3.76
	79	21	3.76
	79	21	3.76
	80	20	4.00
	75	25	3.00
	73	27	2.70
	75	25	3.00

Table 6. Normalised EPMA data (wt.%.) of aurostibite from 560FWD, Hera mine (complete EPMA results in Supplementary Table S1).

Grain	Au	As	Bi	Sb
1	43.06	0.23	0.27	56.45
2	42.87	0.25	0.26	56.63
3	43.18	0.25	0.20	56.38
4	43.42	0.21	0.33	56.04
5	43.61	0.23	0.24	55.91
6	42.98	0.23	0.32	56.47
7	43.40	0.27	0.27	56.06
8	43.41	0.27	0.30	56.03
9	43.54	0.25	0.30	55.92
10	43.68	0.27	0.28	55.78
11	42.92	0.28	0.28	56.52
12	42.82	0.28	0.34	56.56

The upper temperature stability limit for aurostibite has been suggested to be 353°C (Gather *et al.*, 1976 cited in Wang *et al.*, 2009), though an earlier paper by Barton (1971) suggested that it was below 125°C. However, gudmundite is associated with aurostibite at Hera and Williams-Jones and Norman (1997) have suggested that gudmundite is only stable below 300°C. This later

temperature would fit with the chlorite–talc–biotite–actinolite–tremolite–chamosite retrograde skarn assemblage that the aurostibite from Hera is associated with. For the Krasna Hora deposit, Zacharias and Nemec (2017) suggested that aurostibite formed by interaction of pre-existing gold with Sb-rich hydrothermal
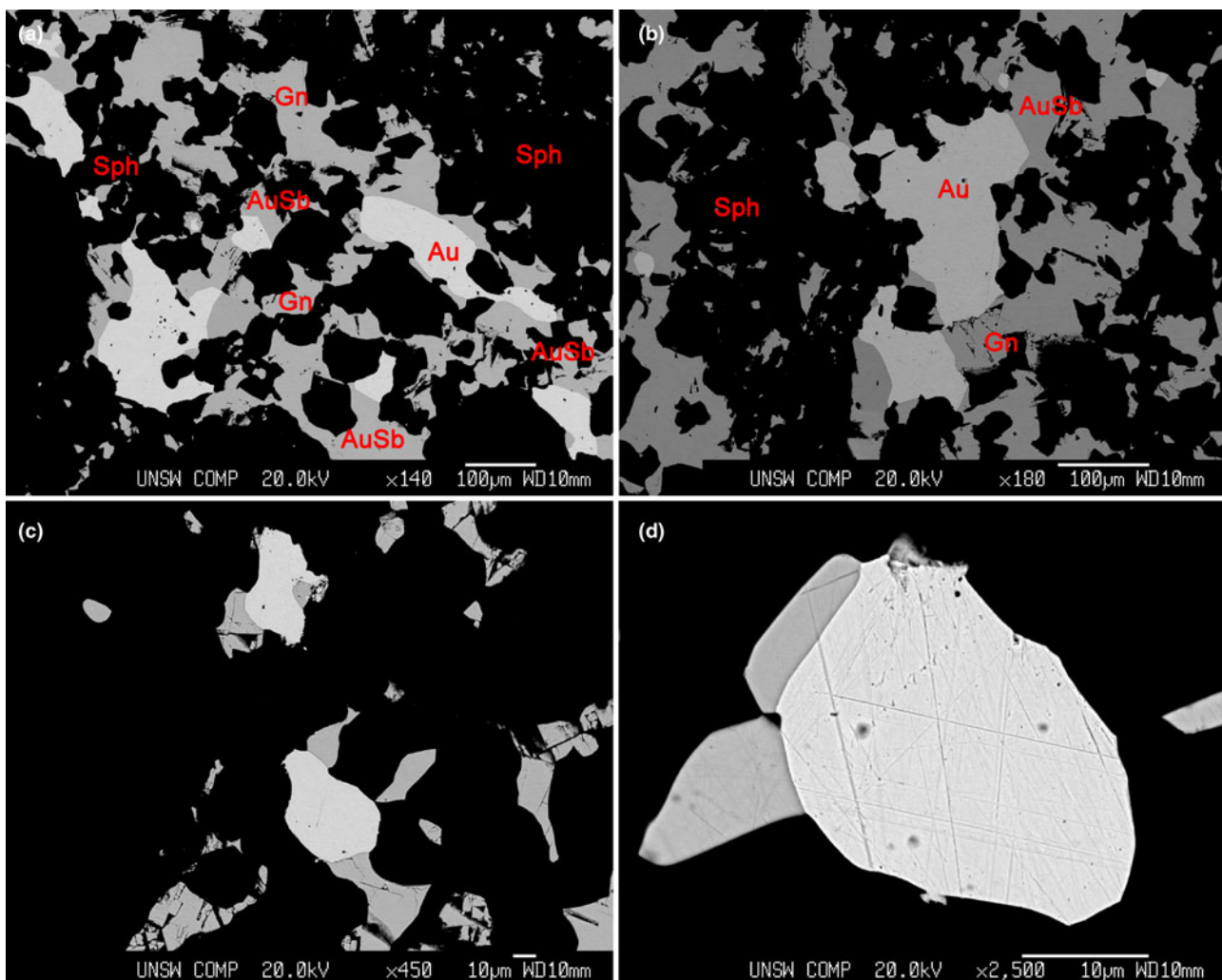
Fig. 6. Back-scatter electron images of the aurostibite–gold association from 560 FWD: (a) network textured gold (white, Au) rimmed by aurostibite (AuSb) and galena (brighter grey, Gn) in sphalerite (dark, Sph); (b) network textured gold (white, Au) rimmed by aurostibite (AuSb) and galena (brighter grey, Gn) in sphalerite (dark, Sph); (c) gold (bright white) rimmed by aurostibite (palest grey); and (d) equant-shaped gold grain rimmed by subhedral aurostibite grains.

Table 7. Relationships between gold–silver ratios and mineral associations.

Ore Body	Sample	Au:Ag	Analyses	Associations
Main	385NOD2	96:4	12	Gold in host-rock with minor disseminated galena, pyrrhotite, chalcopyrite clinochlore, quartz and muscovite
Far West	560FWD	89:11	27	Aurostibite rimming gold in galena and sphalerite
		88:12	21	Minor gudmundite and tetrahedrite, rare pyrrhotite and chalcopyrite
		87:13	1	Clinochlore, talc, biotite, actinolite, tremolite and chamosite
Far West Deeps	535XC	80:20	2	Gold in sphalerite–galena intergrowths
		79:21	3	Aligned gold grains in sphalerite cross-cutting earlier sphalerite–galena
		75:25	2	Quartz, tremolite, clinochlore and zoisite
		73:27	1	
Main South	335XC	46:54	3	Gold within galena, pyrrhotite and sphalerite
				Minor chalcopyrite and tetrahedrite, rare pyrite
				Quartz, muscovite, K-feldspar and chlorite
Central South	HRUD497	42:58	2	Massive sphalerite cross-cut by gold–galena–nisbite
				Gold rimmed by galena–gudmundite–chalcopyrite in sphalerite
				Minor pyrrhotite, tetrahedrite, native Sb and rare pyrite
				Quartz, clinochlore, tremolite, K-feldspar, muscovite, biotite and zoisite
North Pod	HRUD470b	38:62	5	Electrum associated with chalcopyrite, breithauptite, dyscrasite, galena and pyrrhotite
		37:63	4	Pyrrhotite rimming electrum
		29:71	5	Sphalerite, minor gudmundite and tetrahedrite
		28:72	4	Clinochlore, zoisite, quartz and tremolite
		27:73	2	

fluids. The textural and chemical evidence from Hera suggests a similar model and that during the formation of aurostibite from gold, the released silver from the host gold reacted with Sb-rich hydrothermal fluids leading to the late-stage formation of tetrahedrite-(Fe), argentotetrahedrite-(Fe), native silver, acanthite and dyscrasite (Graham *et al.*, 2021), all of which are post-gold in formation.

Evidence for multiple generations of gold mineralisation

Remobilisation involves the physical and/or chemical translocation and disassociation of sulfides and/or wallrock from their original sites of formation (Marshall and Gilligan, 1987). The textural evidence for remobilisation includes recrystallisation of sulfides, mixed breccia sulfide-silicate ores, boudinage, foliations, elongation lineations and folding of sulfide layers (Gilligan and Marshall, 1987). Almost all of these are present within the Hera deposit, and are especially evident within the Sb-rich Far West and North Pod ore bodies (Burrows, 2017; Lay *et al.*, 2019; Schellen, 2019).

The almost complete lack of correlation between gold and other metals assayed for (Table 2), along with the gold from differing sulfide lenses correlating weakly with different elements (i.e. the best, though still weak, correlations being with sulfur for Far West and Far West Deeps, Ag with Main North and Main South and with Cu for North Pod; Table 3) alone suggests that there were multiple gold mineralising events/geochemical overprints at Hera. These correlation coefficients for the assay data also show that much of the gold at Hera is unrelated to the Pb–Zn–Ag mineralisation with these three metals all having a relatively high correlation coefficient with each other (0.82 for Pb–Zn, 0.51 for Pb–Ag and 0.46 for Zn–Ag; Tables 2 and 3).

At Hera, gold varies widely in composition, though mostly between the differing sulfide lenses, generally with little variation within ore bodies. The most Au-rich grains average 95 wt.% Au (Table 4), are restricted to the Main ore body and occur within the host metasiltstone associated with minor galena, pyrrhotite and chalcopyrite and chlorite–muscovite–quartz alteration (Fig. 4a, Table 7). Based on the textural relationships, associations

and chemistry of this occurrence, this is the most likely representative of the initial gold mineralisation at Hera. Gold from the 535XC (Far West Deeps) is also Au rich, though with more widely varying contents, from 73–80 wt.% Au (Table 5). It occurs as aligned grains in a sphalerite vein which cross-cuts an earlier sphalerite–galena vein (Fig. 4b) or as grains within sphalerite. Here, the gold and sulfides are associated with a retrograde skarn alteration assemblage of quartz–tremolite–chlorite–zoisite (Table 7). Gold from a shallower level of the Main South lode (335XC) is far more Ag rich, averaging 46 wt.% Au and thus is electrum (Table 5). Here, the gold occurs within galena, pyrrhotite and sphalerite (Fig. 5e) and is associated with minor chalcopyrite, tetrahedrite-(Fe), rare pyrite and an alteration assemblage of quartz–muscovite–K-feldspar–chlorite (Table 7).

The other gold occurrences studied at Hera are all Sb rich and associated with retrograde skarn assemblages. Gold rimmed by aurostibite from the Far West varies little in composition and averages 87 wt.% Au (Table 4). It is associated with galena and sphalerite, along with minor gudmundite and tetrahedrite-(Fe) and rare pyrrhotite and chalcopyrite (Figs 5 a–d). The associated alteration comprises a retrograde skarn assemblage of chlorite–talc–biotite–tremolite–actinolite–chamosite (Table 7). Gold from the Central South lode (HRUD497) is rich in Ag (42 wt.% Au; Table 4) and hence electrum. It occurs in micro-veinlets of cuspate–lobate gold, galena and nisbite which cross-cut massive sphalerite (Fig. 4c) and in some occurrences is rimmed by galena, gudmundite and chalcopyrite (Fig. 4d). In places, it is also associated with minor pyrrhotite, tetrahedrite-(Fe), native antimony and rare pyrite. This occurrence has a partly retrograde skarn alteration assemblage of quartz–chlorite–tremolite–K-feldspar–muscovite–biotite–zoisite (Table 7). The most Ag-rich gold samples from Hera are from the North Pod with 26.77–37.55 wt.% Au (Table 4) and hence electrum. Electrum from here is associated with breithauptite, dyscrasite, chalcopyrite, galena and pyrrhotite, along with minor sphalerite, gudmundite, tetrahedrite-(Fe) and argentotetrahedrite-(Fe) (Figs 4e and f). It occurs with a retrograde skarn assemblage of chlorite–zoisite–tremolite–quartz (Table 7). Based on their textural relationships, ore mineral assemblages and associated retrograde skarn alteration assemblages,
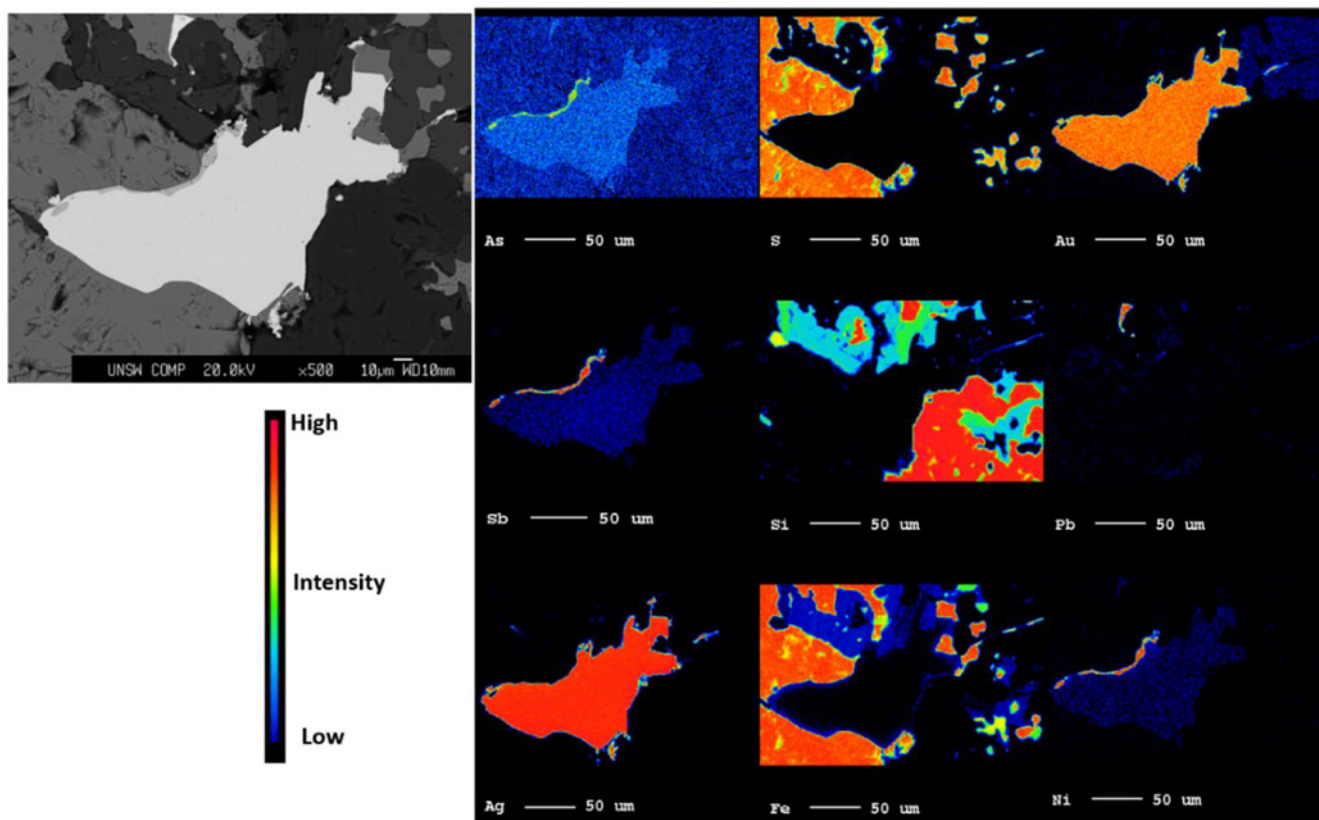
Fig. 7. WDS element map of electrum partially rimmed by breithauptite within pyrrhotite (HRUD470) from the North Pod.

these Sb-rich gold occurrences probably represent a final stage of gold mineralisation at Hera. In all these occurrences, the gold grains are rimmed by later Sb-rich phases and this is clearly shown in the WDS element map in Fig. 7 where an electrum grain is rimmed by breithauptite with a very sharp contact between the two phases and all Au and Ag restricted to the electrum grain. For the Suzdal sediment-hosted gold deposit of Eastern Kazakhstan, Kovalev *et al.* (2009) found that aurostibite along with other Sb-phases and rare Ni–Co–As–Sb phases in close association with gold were indicative of remobilisation. The same can be applied to Hera as exemplified by the occurrence of aurostibite, breithauptite and nisbite as rims around gold grains.

A histogram showing the wt.% Au versus number of analyses (Fig. 8) clearly shows five main peaks of gold compositions: 28–37 (HRUD470b from North Pod), 42–46 (HRUD497 from Central South and 335XC from Main South), 75–86 (560FWD from Far West and 535XC from Far West Deeps), 87 (560FWD from Far West Deeps) and 95–96 (385NOD from Main lode). The peak at 87 wt.% Au is skewed by the number of analyses from this sample though is consistent with the other analyses from this lode at ~86 wt.% Au. The spatial distribution of these (see Fig. 2) would suggest that gold from the centre of the deposit is distinctly more Au rich compared to gold from the margins of the deposit, though more analyses would be required to support this.

A number of authors have suggested that primary gold with higher Ag contents correlates with lower temperatures of formation (Morrison *et al.*, 1991; Gammons and Williams-Jones, 1995). More recently, Bonev *et al.* (2002) suggested this for gold from the Chelopech epithermal Au–Cu deposit of Bulgaria.

This is certainly reflected at Hera (Table 7) with the first stage of gold mineralisation in the host-rock having the highest Au: Ag (96:4) and presumably occurring at the highest temperature, along with gold associated with Sb phases with the lowest Au: Ag (42:58 down to 27:73) reflecting lower temperatures of formation. If this holds true, then a progression from the highest temperature to lowest temperature ore lenses for Hera would be Main (96:4), Far West (~89:11), Far West Deeps 535XC (80:20 to 73:27), Main South 335XC (46:54), Central South (42:58) and finally North Pod (38:62 to 27:73). For at least the Main South lense, this would also suggest that higher silver content reflects decreasing temperature with elevation. Although EPMA results for gold with antimony are only rarely reported in the literature as such a chemistry is likely to be of rare occurrence (Hough *et al.*, 2009), Ciobanu *et al.* (2010) found that gold associated with maldonite from Maldon, Victoria, Australia contained small amounts of antimony (up to 0.04 wt.%). In addition, the recent paper of Chapman *et al.* (2021), though failing to mention antimony in gold via EPMA, found substantial antimony in gold using laser ablation inductively coupled plasma mass spectrometry in the orogenic gold deposits they investigated. Thus, the relatively high Sb (1.05–2.71 wt.%) content within electrum from the North Pod and Central South lenses may not be restricted solely to gold–antimony occurrences and is possibly indicative (though experimental work would be required to prove this) of a lower temperature of formation during the terminal stages of retrogressive metamorphism.

For the Krasna Hora deposit, based on fluid inclusion and experimental data, Zacharias and Nemec (2017) and Nemec and Zacharias (2018) suggested that gold formed at temperatures
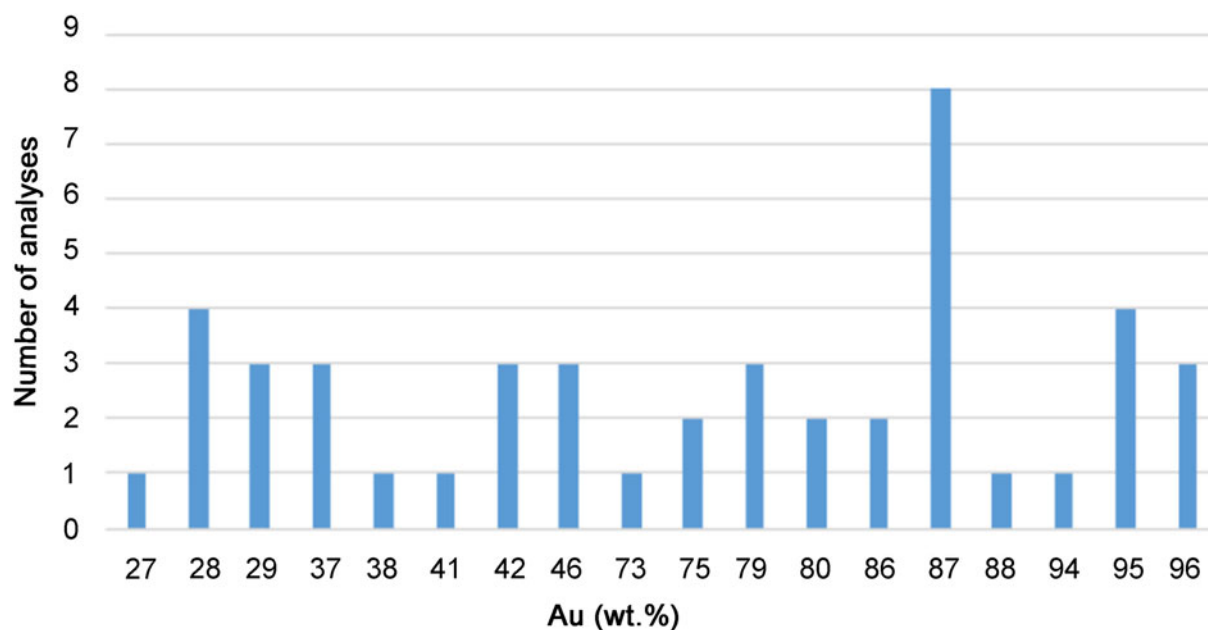
Fig. 8. Histogram showing wt.% Au of the gold and/or electrum grains versus number of analyses.

of ~130–170°C. Important and relevant to this study, they also found four generations of gold, with Au-1 (1.99–10.36 wt.% Ag) being the most abundant and associated with calcite; Au-2 (15.70–48.16 wt.% Ag) forming narrow zones or rims around Au-1; Au-3 (~0 wt.% Ag and only found in one sample) as thin replacements of both Au-1 and Au-2 and Au-4 (< 5 at.% Ag) as a spongy and probable supergene phase. Many hydrothermal gold deposits have multiple generations of gold formation (e.g. Lapa mine, Canada, Simard *et al.*, 2013; Kharma deposit of Bolivia, Dill *et al.*, 1995; Mokrsko-West deposit of the Bohemian Massif, Czech Republic, Zacharias *et al.*, 2014) and the Hera deposit is no exception to this. For deposits subjected to metamorphism (e.g. see Marshall and Gilligan, 1987; Cook, 1996 amongst others) after any early stage of mineralisation, such as for the Hera deposit, the differing generations of gold and other metals can be ascribed to remobilisation events during subsequent metamorphism. For Hera, most of this remobilisation probably occurred during widespread retrogressive metamorphism as shown by the alteration assemblages associated with each of the ore lenses, at temperatures below 300°C.

Although a number of quartz vein generations are relatively widespread throughout the Hera deposit, only the late-stage coarse-grained quartz carries any mineralisation, in the form of relatively coarse-grained (>10 mm) pyrrhotite, chalcopyrite, cubanite, galena and sphalerite. None of the generations of quartz veins from Hera have been found to contain any gold. In terms of the hydrothermal fluid source, although granites are relatively widespread in the region, these are significantly older than the Hera deposit (~382 Ma) having been dated to 428–422 Ma (Chisolm *et al.*, 2014; Waltenberg *et al.*, 2019). However, Graham *et al.* (2021) described granite pegmatite dykes, comprising intergrowths of microcline–anorthite–albite–quartz, which cross-cut both the host-rock sequence and sulfide lenses on levels 285SB, 285SC, 310SA and 615FWA. These may be related to an underlying magmatic body responsible for both the source of the skarn-forming fluids and some of the metals at Hera, especially Sb, As and Bi.

Conclusions

Gold correlates poorly with other metals across the Hera deposit and also between the various ore lenses. The deposit contains a number of distinctive gold associations, each with a distinctive gold chemistry. These span a wide range from early host-rock associated gold comprising 96 wt.% Au, through intermediate gold compositions (86–73 wt.% Au) associated with base-metal sulfides to Ag-rich electrum (42–27 wt.% Au) associated with a number of Sb phases and retrogressive skarn alteration. Aurostibite with a homogenous composition was found to rim gold with the gold itself containing no antimony but 11–12 wt.% Ag. This aurostibite formed via interaction of Sb-rich hydrothermal fluids (associated with retrogressive skarn formation) with pre-existing gold. The wide range in gold compositions and associations is attributed to widespread physical and chemical remobilisation associated with multiple periods of deformation, principally in the form of shear zones and faults. Sb-rich gold may be indicative of a low temperature of formation during the terminal phases of metamorphism and may be more common in orogenic gold deposits than previously thought.

References

Ashley P.M., Creagh C.J. and Ryan C.G. (2000) Invisible gold in ore and mineral concentrates from the Hillgrove gold-antimony deposits, NSW, Australia. *Mineralium Deposita*, **35**, 285–301.

Aurelia Metals Ltd (2018) *Hera/Nymagee Resources and Reserves*. ASX announcement (unpubl. Rep). Aurelia Metals Ltd., Brisbane, Australia [Available at https://www2.asx.com.au/markets/trade-our-cash-market/announcements.ami, 17 Jul 2018].

Barton P.B. Jr. (1971) The Fe–Sb–S system. *Economic Geology*, **66**, 121–132.

Biagioni C., George L.L., Cook N.J., Makovicky E., Moelo Y., Pasero M., Sejkora J., Stanley C.J., Welch M.D. and Bosi F. (2020) The tetrahedrite group: Nomenclature and classification. *American Mineralogist*, **105**, 109–122.

Bonev I.K., Kerestedjian T., Atanassova R. and Andrew C.J. (2002) Morphogenesis and composition of native gold in the Chelopech volcanic-hosted Au-Cu epithermal deposit, Srednogorie zone, Bulgaria. *Mineralium Deposita*, **37**, 614–629.

Boyle R.W. (1979) *The Geochemistry of Gold and its Deposits*. Geological Survey of Canada Bulletin 280, 584p. Geological Survey of Canada, Ottawa.

Bryzgalov I.A., Krivitskaya N.N. and Spiridonov E.M. (2007) First finding of nisbite and aurostibite in the Eastern Transbaikal region. *Doklady Earth Sciences*, **417**, 1265–1267.

Burrows L. (2017) *Comparison of the ore and gangue mineralogy and metal ratios for the different ore lenses of the Hera Mine, Central NSW*. University of New South Wales Sydney, Honours Thesis (unpublished), Australia.

Cabri L.J., Hoy D., Rudashevsky N.S. and Rudashevsky V.N. (2007) Mineralogical evaluation of Au–Sb–As mineralization from the AD-MW zones, Clarence Steam property, New Brunswick. Paper 30, *39*[th] *Annual Meeting of the Canadian Mineral Processors*, Ottawa, Ontario, Canada, 517–533.

Chapman R.J., Leake R.C., Bond D.P., Stedra V. and Fairgrieve B. (2009) Chemcial and mineralogical signatures of gold formed in oxidizing chloride hydrothermal systems and their significance within populations of placer gold grains collected during reconnaissance. *Economic Geology*, **104**, 563–585.

Chapman R.J., Banks D.A., Styles M.T., Walshaw R.D., Piazolo S., Morgan D.J., Grimshaw M.R., Spence-Jones C.P., Matthews T.J. and Borovinskaya O. (2021) Chemical and physical heterogeneity within native gold: implications for the design of gold particle studies. *Mineralium Deposita*, **56**, 1563–1588.

Chisolm E.I., Blevin P.L., Downes P.M. and Simpson C.J. (2014) New SHRIMP U–Pb zircon ages from the central Lachlan Orogen and Thomson Orogen, New South Wales: July 2011–June 2012. *Geoscience Australia Canberra Record 2014/32, Geological Survey of New South Wales Record GS 2013/1837*, Geoscience Australia, Canberra, Australia.

Ciobanu C.L., Birch W.D., Cook N.J., Pring A. and Grundler P.V. (2010) Petrogenetic significance of Au-Bi-Te-S associations: The example of Maldon, Central Victorian Gold Province, Australia. *Lithos*, **116**, 1–17.

Cook N.J. (1996) Mineralogy of the sulphide deposits at Sulitjelma, northern Norway. *Ore Geology Reviews*, **11**, 303–338.

Cook N.J., Halls C. and Boyle A.P. (1993) Deformation and metamorphism of massive sulphides at Sulitjelma, Norway. *Mineralogical Magazine*, **57**, 67–81.

David V. (2005) *Structural Setting of Mineral Deposits in the Cobar Basin*. PhD thesis (unpublished), University of New England, Armidale, NSW, Australia.

David V. (2006) Cobar Superbasin System metallogenesis. Pp. 39–51 in: *Mineral Exploration Geoscience in New South Wales Extended Abstracts, Mines and Wines Conference*, Mineral Exploration Discussion Group (SMEDG), Cessnock, NSW, Australia.

David V. (2018) Cobar Deposits – structural control. *Australian Society for Exploration Geophysics (ASEG) Extended Abstracts*, **2018**:1, 1–9.

Desborough G.A. (1970) Silver depletion indicated by microanalysis of gold from placer occurrences, western United States. *Economic Geology*, **65**, 304–311.

Deschenes G., Xia C., Fulton M., Cabri L.J. and Price J. (2009) Determination of the leaching parameters for a refractory gold ore containing aurostibite and antimony minerals: Part II – AD Zone. *Minerals and Metallurgical Processing*, **26**, 114–120.

Dill H.G., Weiser T., Bernhardt I.R. and Riera Kilibarda C. (1995) The composite gold-antimony vein deposit at Kharma (Bolivia). *Economic Geology*, **90**, 51–66.

Downes P.M. and Phillips D. (2018) [40]Ar/[39]Ar dating of three samples from mineralized zones in the Nymagee project area: Preliminary results. In: *Geological Survey of New South Wales Report GS2018/0164*, Geological Survey of New South Wales, Maitland, Australia.

Fisher N.H., (1945) The fineness of gold, with special reference to the Morobe gold field, New Guinea. *Economic Geology*, **40**, 449–495.

Fitzherbert J., Mawson R., Mathieson D., Simpson A., Simpson C. and Nelson M. (2017) Metamorphism in the Cobar Basin: current state of understanding and implications for mineralisation. *Quarterly Notes of the New South Wales Geological Survey*, **148**, 1–35.

Fitzherbert J.A., McKinnon A.R., Blevin P.L., Waltenburg K., Downes P.M., Wall C., Matchan E. and Huang H. (2020) The Hera orebody: A complex distal (Au–Zn–Pb–Ag–Cu) skarn in the Cobar Basin of central New South Wales, Australia. *Resource Geology*, **2021**, 1–24, DOI: 10.1111/rge.12262

Frimmel H.E. (2014) A giant Mesoarchean crustal gold enrichment episode: possible causes and consequences for exploration. In: *Building Exploration Capability for the 21*[st] *Century* (Kelley, K.P. and Golden, H.C., editors). Special Publication 18, Society of Economic Geologists, Colorado, USA.

Gammons C.H. and Williams-Jones A. (1995) The solubility of Au Ag alloy +AgCl in HCl/NaCl solutions at 300°C: new data on the stability of Au (1) chloride complexes in hydrothermal fluids. *Geochimica et Cosmochimica Acta*, **59**, 3453–3468.

Gathers G.R., Shanes J.W. and Brier M.C. (1976) Improved apparatus for thermophysical measurements on liquid metals up to 8000K. *Review of Scientific Instruments*, **47**, 471–479.

Gilligan L.B. and Marshall B. (1987) Textural evidence for remobilization in metamorphic environments. *Ore Geology Reviews*, **2**, 205–229.

Glen R.A. (1990) Formation and inversion of transtensional basins in the western part of the Lachlan Fold Belt, Australia, with emphasis on the Cobar Basin. *Journal of Structural Geology*, **12**, 601–620.

Glen R. (1991) Inverted transtensional basin setting for gold and copper and base metal deposits at Cobar, New South Wales. *BMR Journal of Australian Geology and Geophysics*, **12**, 13–24.

Glen R., Dallmeyer R. and Black L. (1992) Isotopic dating of basin inversion—the Palaeozoic Cobar basin, Lachlan orogen, Australia. *Tectonophysics*, **214**, 249–268.

Glen R.A., Drummond B.J., Goleby B.R., Palmer D. and Walce-Dyste K.D. (1994). Structure of the Cobar Basin, New South Wales, based on seismic reflection profiling. *Australian Journal of Earth Sciences*, **41**, 341–357.

Graham A.R. and Kaiman S. (1952) Aurostibite, AuSb$_2$: a new mineral in the pyrite group. *American Mineralogist*, **37**, 461–469.

Graham I.T., McKinnon A., Schellen K., Lay A., Liepa E., Burrows L., Privat K., Quan H., French D. and Dietz C. (2021) Hera: evidence for multiple mineralization events and remobilization in a sediment-hosted Au-Pb-Zn-Ag deposit, central New South Wales, Australia. *Environmental Sciences Proceedings*, **6**, 28.

Harris D.C. (1990) The mineralogy of gold and its relevance to gold recoveries. *Mineralium Deposita*, **25**, S3–S7.

Hough R.M., Butt C.R.M. and Fischer-Buhner J. (2009) The crystallography, metallography and composition of gold. *Elements*, **5**, 297–302.

Ispolatov V., Lafrance B., Dube B., Creaser R. and Hamilton M. (2008) Geologic and structural setting of gold mineralization in the Kirkland Lake – Larder Lake Gold Belt, Ontario. *Economic Geology*, **103**, 1309–1340.

Jebrak M., Lebrun C., Andre-Mayer A-S. and Simard M. (2016) Native antimony emplaced by methane-rich hydrothermal fluid in an orogenic fault-zone. *Terra Nova*, **29**, 401–408.

Jedwab J. and Mendes Chuva J. (1992) Reflected-light microscope and SEM/EMP observations on the behaviour of aurostibite (AuSb$_2$) during amalgamation. *Mineralogical Magazine*, **56**, 561–565.

Kalinin A.A., Savchenko Y. and Selivanova E.A. (2019) Mustard gold in the Oleninskoe gold deposit, Kolmozero-Voronya greenstone belt, Kola Peninsula, Russia. *Minerals*, **9**, 786.

Knight J.B., Mortensen J.K. and Morison S.R. (1999) Lode and placer gold composition in the Klondike District, Yukon Territory, Canada: Implications for the nature and genesis of Klondike placer and lode gold deposits. *Economic Geology*, **94**, 649–664.

Kontak D.J., Horne R.J. and Smith P.K. (1996) Hydrothermal characterisation of the West Gore Sb-Au deposit, Meguma Terrane, Nova Scotia, Canada. *Economic Geology*, **91**, 1239–1262.

Kovalev K.R., Kalinin Y.A., Naumov E.A., Pirajno F. and Borisenko A.S. (2009) A mineralogical study of the Suzdal sediment-hosted gold deposit, Eastern Kazakhstan: implications for ore genesis. *Ore Geology Reviews*, **35**, 186–205.

Lawrie K. and Hinman M. (1998) Cobar-style polymetallic Au–Cu–Ag–Pb–Zn deposits. *AGSO Journal of Australian Geology and Geophysics*, **17**, 169–187.

Lay A. (2019) *A Comparative Study of the Mineralogy And Geochemistry of Ore Minerals from Silver-Rich Polymetallic Deposits of the Lachlan and Southern New England Orogens, New South Wales, Australia*. PhD Thesis (unpublished), University of New South Wales, Australia.

Lay A., Graham I., Burrows L., McKinnon A. and Privat K. (2018) Ore and Gangue Minerals of the Hera Au-Pb-Zn-Ag Deposit, Cobar Basin, NSW. *Australian Society of Exploration Geophysics* (*ASEG*) *Extended Abstracts*, **2018**(1), 1–7.

Liepa E.A.C. (2019) *Vectoring Towards Mineralisation: An Investigation into the Regional Geochemical and Mineralogical Trends Toward the Hera Ore Deposit of the Cobar Basin, Central NSW*. Honours Thesis (unpublished), University of New South Wales Sydney, Australia.

Liu H., Beaudoin G., Makvandi S., Jackson S.E. and Huang X. (2021) Multivariate statistical analysis of trace element compositions of native gold from orogenic gold deposits: implication for mineral exploration. *Ore Geology Reviews*, **131**, 1–17.

Marshall B.M. and Gilligan L.B. (1987) An introduction to remobilisation: information from ore-body geometry and experimental considerations. *Ore Geology Reviews*, **2**, 87–131.

McKinnon A.R. and Fitzherbert J.A. (2017) New Developments at the Hera Au-Pb-Zn-Ag Mine, Nymagee, New South Wales. *Discoveries in the Tasmanides*. *AIG Bulletin*, **67**, 1–14.

Milesi J.P., Toteu S.F., Deschamps Y., Feybesse J.L., Lerouge C., Cocherie A., Penaye J., Tchameni R., Moloto-A-Kenguemba G., Kampunzu H.A.B., Nicol N., Duguey E., Leistel J.M., Saint-Martin M., Ralay F., Heinry C., Bouchot V., Doumnang Mbaigane J.C., Kanda Kula V., Chene F., Monthel J., Boutin P. and Cailteux J. (2006) An overview of the geology and major ore deposits of Central Africa: Explanatory note for the 1:4,000,000 map 'Geology and major ore deposits of Central Africa'. *Journal of African Earth Sciences*, **44**, 571–595.

Missen O.P., Etschmann B., Mills S.J., Sanyal S.K., Ram R., Shuster J., Rea M.A.D., Raudsepp M.J., Fang X-Y., Lausberg E.R., Melchiorre E., Dodsworth J., Liu Y., Wilson S.A. and Brugger J. (2022). Tellurium biogeochemical transformation and cycling in a metalliferous semi-arid environment. *Geochimica et Cosmochimica Acta*, **321**, 265–292.

Morrison G.W., Rose W.J. and Jaireth S. (1991) Geological and geochemical controls on the silver content (fineness) of gold in gold-silver deposits. *Ore Geology Reviews*, **6**, 333–364.

Nemec M. and Zacharias J. (2018) The Krasna Hora, Milesov, and Pricovy Sb-Au deposits, Bohemian Massif: mineralogy, fluid inclusions, and stable isotope constraints on the deposit formation. *Mineralium Deposita*, **53**, 225–244.

Novoselov K., Belogub E., Kotlyarov V. and Mikhailov A. (2015) Ore mineralogy and formation conditions of the Pirunkoukku gold occurrence (Finland). *European Journal of Mineralogy*, **27**, 639–649.

Oberthur T. and Weiser T.W. (2008) Gold-bismuth-telluride-sulphide assemblages at the Viceroy Mine, Harare-Bindura-Shamva greenstone belt, Zimbabwe. *Mineralogical Magazine*, **72**, 953–970.

Pasero M. (2022) *The New IMA List of Minerals*. International Mineralogical Association. Commission on new minerals, nomenclature and classification (IMA-CNMNC). http://cnmnc.main.jp/ [Accessed 11.05.2022].

Ravanelle J-F., Lutes G.G. and Hynes A.J. (2008) Architecture of gold mineralization at Anomaly A of the Clarence Stream Deposits, Southern New Brunswick. *Exploration and Mining Geology*, **17**, 85–100.

Schellen K. (2019) *Comparison of the Ore and Gangue Mineralogy for the Different Ore Lenses of the Hera Mine, Central NSW*. BEES0006 Report (unpublished), University of New South Wales Sydney, Australia.

Schellen K. (2020) *Comparison of the Ore and Gangue Mineralogy, Metal Ratios and Hostrock Sequences Between the Newly-Discovered Federation Deposit and the Hera Mine, Central NSW*. Honours Thesis (unpublished), University of New South Wales Sydney, Australia.

Shelton K.L., McMenamy T.A., van Hees E.H.P. and Falck H. (2004) Deciphering the complex fluid history of a greenstone-hosted gold deposit: fluid inclusion and stable isotope studies of the Giant mine, Yellowknife, Northwest Territories, Canada. *Economic Geology*, **99**, 1643–1663.

Simard M., Gaboury D., Daigneault R. and Mercier-Langevin P. (2013) Multistage gold mineralization at the Lapa mine, Abitibi Subprovince: insights into auriferous hydrothermal and metasomatic processes in the Cadillac-Larder Lake Fault Zone. *Mineralium Deposita*, **48**, 883–905.

Spiridonov E.M., Krivitskaya N.N., Bryzgalov I.A., Kulikova I.M. and Gorodetskaya M.D. (2010) Bismuth-rich aurostibite: a product of maldonite replacement in a volcanogenic-plutonogenic Darasun deposit (Eastern Transbaikalia). *Doklady Earth Sciences*, **435**, 1611–1613.

Townley B.K., Herail G., Maksaev V., Palacios C., de Parseval P., Sepulveda F., Orellana R., Rivas P. and Ulloa C. (2003) Gold grain morphology and composition as an exploration tool: application to gold exploration in covered areas. *Geochemistry, Exploration, Environment, Analysis*, **3**, 29–38.

Vokes F.M. (1969) A review of the metamorphism of sulphide deposits. *Earth-Science Reviews*, **5**, 99–143.

Waltenberg K., Blevin P.L., Hughes K.S., Bull K.F., Fitzherbert J.A., Cronin D.E. and Bultitude R.J. (2019) New SHRIMP U–Pb zircon and titanite ages from the Lachlan Orogen and the New England Orogen, New South Wales. Pp. 58–70 in: *Geoscience Australia Record 2019/05 and Geological Survey of New South Wales Report GS2019/0409*. Mineral Systems Projects, July 2016-June 2017, Geoscience Australia, Canberra, Australia.

Wang J., Leinenbach C. and Roth M. (2009) Thermodynamic description of the Au–Ge–Sb ternary system. *Journal of Alloys and Compounds*, **485**, 577–582.

Watters S., Castonguay S., Lutes G.G. and McLeod M.J. (2008) Gold mineralization at the Anomaly A deposit, Clarence Stream Area, southwestern New Brunswick: distal deposits of a syn-deformational intrusion-related gold system?. *Exploration and Mining Geology*, **17**, 67–84.

Williams-Jones A.E. and Normand C. (1997) Controls of mineral paragenes in the system Fe–Sb–S–O. *Economic Geology*, **92**, 308–324.

Zacharias J. and Nemec M. (2017) Gold to aurostibite transformation and formation of Au–Ag–Sb phases: the Krasna Hora deposit, Czech Republic. *Mineralogical Magazine*, **81**, 989–999.

Zacharias J., Moravek P., Gadas P. and Pertoldova J. (2014) The Mokrsko-West gold deposit, Bohemian Massif, Czech Republic: mineralogy, deposit setting and classification. *Ore Geology Reviews*, **58**, 238–263.